Sodium lanthanide tungstate-based nanoparticles as bimodal contrast agents for *in vivo* high-field MRI and CT imaging

Elisabet Gómez-González,[a,†,*] Carlos Caro,[b,c,†] Nuria O. Núñez,[a] Daniel González-Mancebo,[a] Jesús D. Urbano-Gámez,[b,c] Maria L. Garcia-Martin,[b,c,d] and Manuel Ocaña[a,*]

[a] *Instituto de Ciencia de Materiales de Sevilla (CSIC-US), c/Américo Vespucio, 49, 41092 Sevilla, Spain*

[b] *Biomedical Magnetic Resonance Laboratory-BMRL, Andalusian Public Foundation Progress and Health-FPS, Seville, Spain*

[c] *Instituto de Investigación Biomédica de Málaga y Plataforma en Nanomedicina–IBIMA Plataforma Bionand, C/Severo Ochoa, 35, 29590 Malaga, Spain.*

[d] *Biomedical Research Networking Center in Bioengineering, Biomaterials &Nanomedicine (CIBER-BBN), 28029 Madrid, Spain*

[†] Both authors contributed equally to this work

*Corresponding authors: Manuel Ocaña. E-mail: mjurado@icmse.csic.es and Elisabet Gómez-González: E-mail: elisabet.gomez@icmse.csic.es

Suppementary Information

Methods:

1. Transverse relaxation rate. T_2 values were measured on a Bruker Biospec MRI system (Bruker Biospec, Bruker BioSpin, Ettlingen, Germany) equipped with 400 mT m^{-1} field gradients and a 40 mm quadrature bird-cage resonator at 298 K. T_2 values were measured using a 64-echo Carl-Purcell-Meiboom-Gill (CPMG) imaging sequence (TE values from 7.5 ms to 640 ms). The relaxivity, r_2, at both magnetic fields, was calculated from the slope of the linear fit of the relaxation rate ($1/T_2$) versus the concentration.

Regions of interest (ROIs) were drawn on the first image of the image sequence, and the intensity values extracted and fit to the following equations:

$$M_{XY}(t) = M_0 e^{-TE/T_2}$$

where M_z and M_{xy} are the signal intensities at time TR or TE, and M_0 is the signal intensity at equilibrium.

2. MRI. MRI experiments were carried out on a 9.4 T Bruker Biospec system equipped with 400 mT/m gradients and a 40 mm quadrature bird-cage resonator.

EPR effect evaluation was performed using the following experimental scheme: i) acquisition of high-resolution T_2-weighted images, ii) acquisition of T_2 parametric images (quantitative), iii) intravenous injection of the nanoparticles, v) acquisition of high-resolution T_2-weighted images, and vi) acquisition of T_2 parametric images (quantitative).

High-resolution T_2-weighted images were acquired using a turbo-RARE sequence with respiratory gating (TE = 27 ms, TR = 1000 ms, 4 averages, 156 μm in-plane resolution and 1 mm slice thickness).

Quantitative T_2 measurements were performed using a multi-echo spin-echo CPMG sequence (TEs ranging from 7 ms to 448 ms, TR = 3500 ms, FOV = 4 cm, matrix size = 128x128, slice thickness = 1 mm).

The T_2 pharmacokinetics were followed by using a turbo-RARE sequence with the same parameters indicated above but only 1 average to improve temporal resolution (1 image every 30 seconds).

3. Histology. Extracted tissues were fixed in 4% formaldehyde (Panreac, pH 7 buffered) for 48 h, changing the 4% formaldehyde after 24 h. Then, the samples were dehydrated through graded ethanol and embedded in paraffin (temperature 56° C for 2 h under stirring and vacuum). The detailed procedures are described below.

Haematoxylin and Eosin (H&E): paraffin-embedded samples were sectioned at 7 µm thickness, then deparaffinized, rehydrated and stained with H&E, and then dehydrated in ascending concentrations of ethanol, cleared in xylene, and mounted on commercial glass slides.

Results:

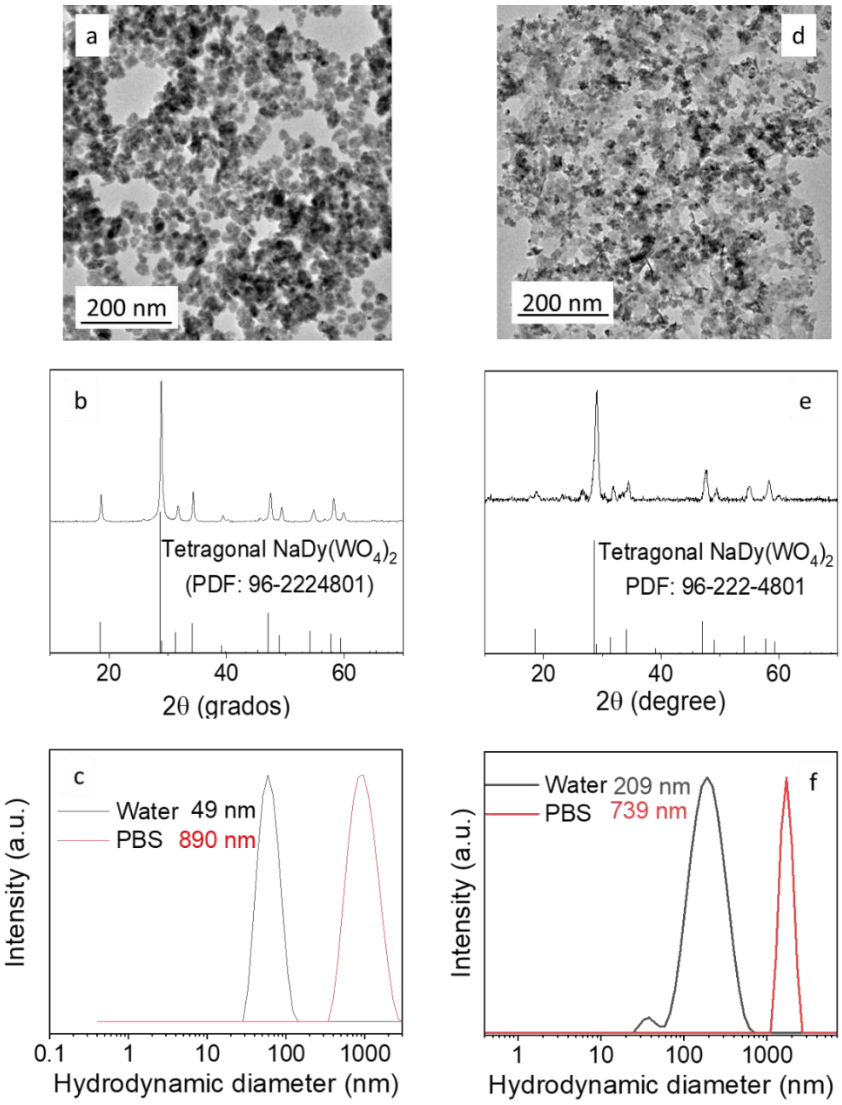

Fig S1. TEM micrograph (a), XRD pattern (b), and DLS curves in water and PBS dispersions (c) of $NaDy(WO_4)_2$ NPs synthesized under the same conditions as those used for the NPs shown in Fig. 1a, but without adding PAA. TEM micrograph (d), XRD pattern (e), and DLS curve in water and PBS dispersions (f) of $NaHo(WO_4)_2$ NPs synthesized under the same conditions as those used for the NPs shown in Fig. 1c, but without adding PAA. Bottom ticks in (b and e) correspond to tetragonal $NaDy(WO_4)_2$ (PDF: 96-222-4801).

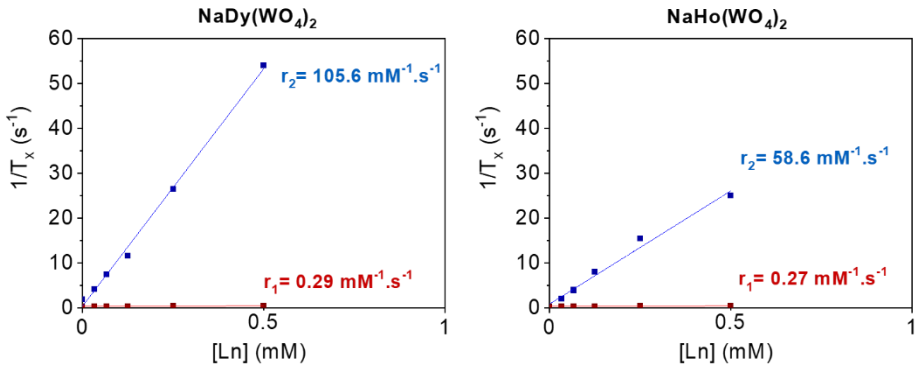

Fig S2. Relaxation rates ($1/T_1$ and $1/T_2$) vs Ln concentration obtained at 9.4 T for aqueous suspensions of $NaDy(WO_4)_2$ and $NaHo(WO_4)_2$ NPs.

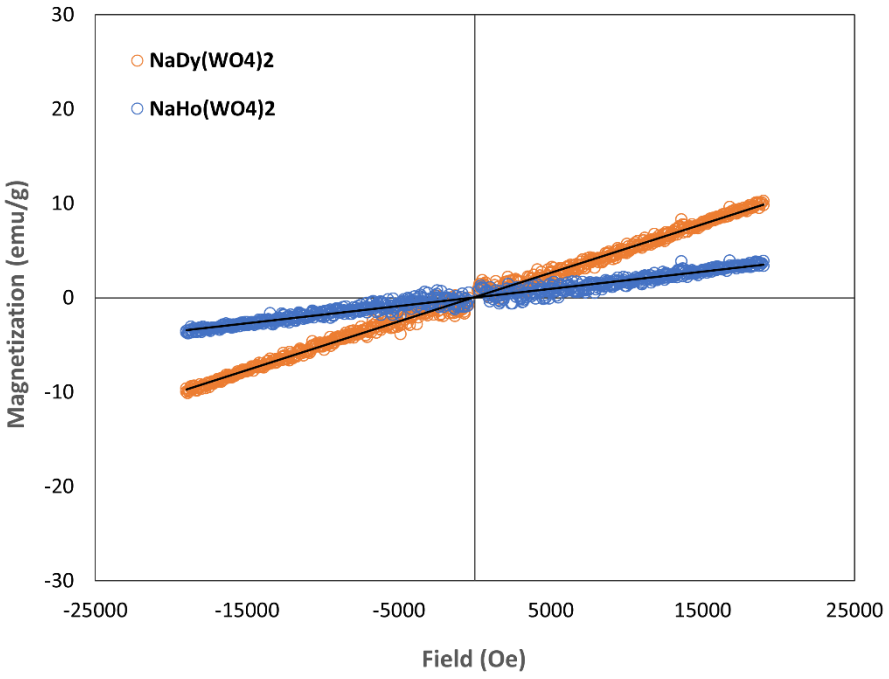

Fig. S3. Magnetization versus applied magnetic field (MvsH) measurements of the NPs at 300 K.

Table S1. r_2 values at 9.4 T reported for different Dy and Ho-based MRI CAs.

Compound	**Size (nm)**	r_2 **($mM^{-1}s^{-1}$)**	**Reference**
HoF_3	70x30	349.98	D. González-Mancebo et al, *Particle & Particle Systems Characterization*, 2017, **34**, 1700116.
HoF_3	110x50	608.39	D. González-Mancebo et al, *Particle & Particle Systems Characterization*, 2017, **34**, 1700116.
DyF_3	110x50	494.24	D. González-Mancebo et al, *Particle & Particle Systems Characterization*, 2017, **34**, 1700116.
$NaDyF_4$	19x25	91.4	X. H. Zhang et al., *Chemistry of Materials*, 2016, **28**, 3060-3072.
$NaHoF_4$	17	130.6	X. H. Zhang et al., *Chemistry of Materials*, 2016, **28**, 3060-3072.
$NaDyF_4$	5.4	32	G. K. Das et al., *Journal of Physical Chemistry Letters*, 2012, **3**, 524-529.
$NaDyF_4$	9.8	51	G. K. Das, et al., *Journal of Physical Chemistry Letters*, 2012, **3**, 524-529.
$NaDyF_4$	20.3	101	G. K. Das et al., *Journal of Physical Chemistry Letters*, 2012, **3**, 524-529.
Dy_2O_3	1.73	11.31	S. Marasini et al., *Bulletin of the Korean Chemical Society*, 2020, **41**, 829-836.
Ho_2O_3	1.7	9.2	S. Marasini et al., *Nanomaterials*, 2021, **11**, 11051355.
$HoPO_4$	27	382.91	E. Gómez-González et al., *Journal of Colloid and Interface Science*, 2021, **587**, 131-140.
$HoPO_4$	48	489.91	E. Gómez-González et al., *Journal of Colloid and Interface Science*, 2021, **587**, 131-140.
$HoPO_4$	80	166.38	E. Gómez-González et al., *Journal of Colloid and Interface Science*, 2021, **587**, 131-140.
$DyPO_4$	23	395	E. Gomez-Gonzalez et al., *Nanoscale*, 2022, **14**, 11461-11470.
$DyPO_4$	37	432	E. Gomez-Gonzalez et al., *Nanoscale*, 2022, **14**, 11461-11470.
$DyPO_4$	57	516	E. Gomez-Gonzalez et al., *Nanoscale*, 2022, **14**, 11461-11470.
$DyVO_4$	66	460.01	E. Gómez-González et al., *Inorganic Chemistry*, 2021, **60**, 152-160.
$HoVO_4$	65	423.68	E. Gómez-González et al., *Inorganic Chemistry*, 2021, **60**, 152-160.
$NaDy(MoO_4)_2$	23	230	E. Gómez-González et al., *Journal of Colloid and Interface Science*, 2023, **629**, 310-321.
$NaDy(MoO_4)_2$	50x16	160	E. Gómez-González et al., *Journal of Colloid and Interface Science*, 2023, **629**, 310-321.
$NaDy(MoO_4)_2$	68x20	198	E. Gómez-González et al., *Journal of Colloid and Interface Science*, 2023, **629**, 310-321.
$NaDy(MoO_4)_2$	87x22	220	E. Gómez-González et al., *Journal of Colloid and Interface Science*, 2023, **629**, 310-321.
$NaDyF_4$@$NaGdF_4$	21.8	147	A.Dash et al., *ACS Appl. Mater. Interfaces*, 2021, **13**, 24345-24355.

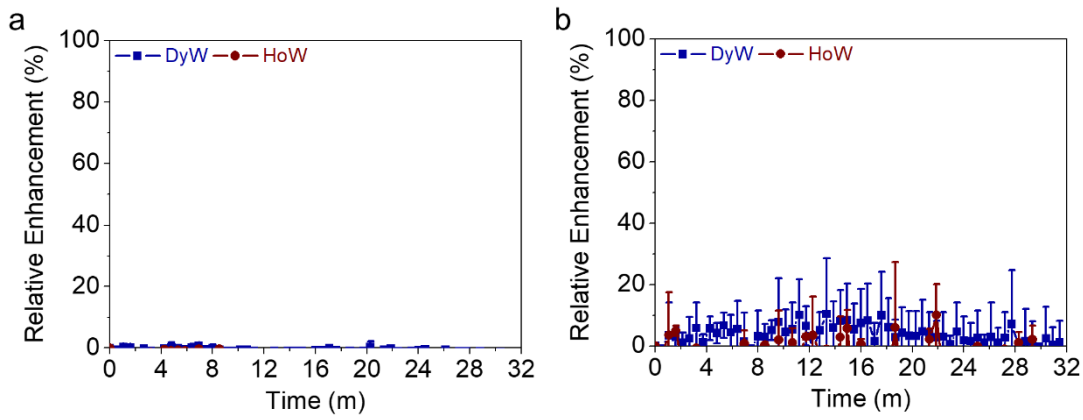

Figure S4. *In vivo* pharmacokinetics of tumor (a) and muscle (b) after the intravenous administration in tumor-bearing mice of $NaDy(WO_4)_2$ NPs (DyW) and $NaHo(WO_4)_2$ NPs (HoW).